ELSEVIER

Cement & Concrete Composites 24 (2002) 89–100

Cement & Concrete Composites

www.elsevier.com/locate/cemconcomp

Effectiveness of concrete inhibitors in retarding rebar corrosion

H. Saricimen *, M. Mohammad, A. Quddus, M. Shameem, M.S. Barry

King Fahd University of Petroleum and Minerals, P.O. Box 1686, Dhahran 31261, Saudi Arabia

Abstract

The effect of inhibitors on the corrosion of steel reinforcements in concrete was evaluated by using anodic polarization, electron spectroscopy for chemical analysis (ESCA) and Auger electron spectroscopy (AES). The reinforcement corrosion in uncontaminated concrete specimens was evaluated by impressing +4 V anodic potential for accelerated corrosion of the steel bar and measuring the time-to-cracking of the concrete specimens. The effectiveness of the inhibitors in retarding reinforcement corrosion in the contaminated concrete specimens was evaluated by measuring the corrosion potentials and corrosion–current density. Results indicated that the time-to-cracking in uncontaminated concrete specimens incorporating inhibitors M2 and R2 was higher than that in the control concrete specimens. While the increase in the time-to-cracking in the concrete specimens incorporating M2 was marginal, a significant improvement in the corrosion-resisting characteristics of concrete incorporating R2 was indicated over the control specimens. The data on time-to-cracking in the uncontaminated concrete specimens and the corrosion rate of steel in the contaminated concrete specimens indicated the usefulness of corrosion inhibitor R2 in retarding reinforcement corrosion. The electrochemical test results and surface analysis results using ESCA and AES techniques showed the better performance of inhibitor R2 compared to inhibitor M2 in retarding corrosion of steel in an environment of saturated calcium hydroxide in the presence of chloride ions.

Keywords: AC impedance spectroscopy; AES; Chloride ions; Concrete; Corrosion; Corrosion potential; Electrochemical; ESCA; Inhibitor; Linear polarization; Reinforcing steel; Saturate calcium hydroxide

1. Introduction

Corrosion of reinforcing steel is the major cause of deterioration of concrete structures in the coastal areas of the Arabian Gulf. The useful service-life of the structures is drastically reduced [1–3] because of this phenomenon. Corrosion of reinforcing steel is mainly attributed to the presence of chloride ions near the concrete–steel interface. The chlorides are generally contributed by the mix constituents – aggregates, admixtures, and mix water. Alternatively, they penetrate the hardened concrete from the service environment – atmosphere, soil, and groundwater.

The soil, groundwater and air in the coastal areas of the Arabian Gulf are contaminated with chloride and sulfate salts [4]. These salts diffuse through the concrete to initiate the deterioration processes. In such a situation, improving the quality of the concrete can extend the service-life of structures. While the production of a dense and impermeable concrete is a first step towards increasing the useful life of structures, other supplementary measures like the use of inhibitors and coated steel bars in concrete constitute an additional precautionary measure to further enhance the durability of structures.

One of the common corrosion prevention practices is to incorporate inhibitors in potentially corrosive environments. Corrosion inhibitors are frequently used in the process industries to inhibit corrosion of the plant components. This technique has also found application in the field of corrosion control of reinforcing steel embedded in concrete likely to be chloride contaminated or exposed to chloride ingress.

The use of inhibitors in concrete was reviewed by Griffin [5], Craig and Wood [6], Treadaway [7], Slater [8] and by Berke [9,10]. In pre-1980 investigations, considerable amount of research was carried out with chromates, phosphates, hypophosphates, alkalis, and fluorides. Craig and Wood [6] studied sodium nitrite, potassium chromate, and sodium benzoate using the polarization technique and found that sodium nitrite

* Corresponding author. Tel.: +966-3-860-6658; fax: +966-3-860-6658.

E-mail address: sarici@kfupm.edu.sa (H. Saricimen).

0958-9465/02/$ - see front matter
PII: S0958-9465(01)00030-0

was the most effective corrosion inhibitor, but it had harmful effects on concrete strength. Similar results were also reported by Treadaway [7] and Treadaway and Russel [11], who found that sodium nitrite inhibited corrosion of steel bars in the presence of chlorides, whereas sodium benzoate did not. Rosenberg et al. [12] studied the effect of calcium nitrite as an inhibitor in reinforced concrete. They used polarization techniques for evaluation of the inhibitors and reported that the relative corrosion rates for samples soaked in saturated sodium chloride solution for 90 d with 2% and 4% admixed calcium nitrite were about a factor of 15 times lower than those without the calcium nitrite admixture. Although stannous chloride also was reported as corrosion inhibitor for reinforcing steel in concrete by Arber and Vivian [13], recent tests by Hope and Ip [14] showed, however, that stannous chloride was not a corrosion inhibitor.

Up to the mid-1970s, the use of inhibitors, due to the above shortcomings, were not appreciated in large scale in concrete. Advances in production of calcium nitrite as a stable solution of up to 40% dissolved solids encouraged its use as a corrosion inhibitor in concrete. Unlike sodium nitrite, in which the sodium cations are detrimental to strength and alkali–aggregate reactions, calcium nitrite was found to be non-detrimental to mechanical properties. Furthermore, later studies showed that calcium nitrite is also compatible with silica fume [15].

In the 1980s, numerous corrosion studies documented the corrosion inhibiting properties of calcium nitrite. The first large-scale results were released in 1983 by the Federal Highway Administration (FHWA) [16]. Even though FHWA used a w/c ratio that was high (>0.5), and added chlorides to the mix water, the conclusion stated that "calcium nitrite can provide more than an order of magnitude reduction in the corrosion rate." The South Dakota Department of Transportation conducted a study in which reinforcing bars were embedded in concrete cylinders with and without admixed chlorides. Cylinders with admixed chlorides went into corrosion immediately (1 d) unless calcium nitrite was present. Samples with calcium nitrite remained passive for 700 d. Calcium nitrite also improved the corrosion resistance of samples without admixed chlorides. Chloride analyses at the reinforcing bar showed that calcium nitrite prevented corrosion at chloride–nitrite ratios of 1.6–2.2 (chloride contents exceeded 10.7 kg/m^3) [16]. Solution experiments by Hope and Ip [14] showed that the ratios of chloride to nitrite can be higher than 11:1.

Berke [17] reported that, after four years of accelerated corrosion with chloride levels at the steel exceeding 7 kg/m^3 (12 lb/yd^2), the only uncorroded specimens were those which contained calcium nitrite.

Japanese research [18] also supported effectiveness of calcium nitrite as a corrosion inhibitor in concrete. In accelerated tests with wetting and drying cycles at 80°C, calcium nitrite was found to be an effective inhibitor for long-term exposures even in marine environment.

Berke and Sundberg [15] showed that the use of calcium nitrite and microsilica should significantly improve the durability of reinforced concrete in marine environment. Studies also showed that calcium nitrite, an anodic inhibitor, modifies the oxide film on the steel bar to be more protective than the film that naturally forms in concrete. The inhibitive action of calcium nitrite depends on its reaction with Fe^{2+} ions according to the following reaction:

$$2Fe^{2+} + 2OH^- + 2NO_2^- \rightarrow 2NO\uparrow + Fe_2O_3 + H_2O$$

Calcium nitrite competes with the chloride ions for ferrous ions produced in concrete and incorporates them into a passive layer on the iron surface, thus preventing further corrosion. Long-term corrosion studies showed that in spite of the decrease in concrete resistivity, corrosion rates were significantly reduced. Likewise, increases in AASHTO T277 chloride permeability values with calcium nitrite were clearly shown to have no negative effects on actual chloride ingress into the concretes [9].

Collins et al. [19] evaluated several inhibitors including (1) a calcium-nitrite-based inhibitor, (2) a monofluorophosphate-based inhibitor, (3) sodium tetraborate ($Na_2B_7O_7 \cdot 10H_2O$), (4) zinc borate ($2ZnO \cdot 3B_2O_3 \cdot 3.5H_2O$), (5) a proprietary oxygenated hydrocarbon produced from an aliphatic hydrocarbon, (6) a proprietary blend of surfactants and amine salts (MCI 2020 which migrate through concrete), and (7) a proprietary alkanolamine inhibitor (MCI 2000). The results of the study, which involved monitoring of corrosion, compressive strength and resistivity, showed that the calcium-nitrite-based inhibitor was the most promising to mitigate corrosion in a repaired structure after removal of chloride-contaminated old concrete. On the other hand, both borate compounds were found to retard the setting of Portland cement.

Prowell et al. [20] further evaluated some of the inhibitors studied by Collins et al. [19] and conducted ponding experiments where they monitored corrosion by measuring half-cell potential, linear polarization resistance, and chloride ion concentration for a period of 325 d. They reported that two proprietary inhibitors Alox 902 and Cortec VCI-337 (MCI 2020) were the best performers.

In the present study proprietary organic- and inorganic-based inhibitors were evaluated under accelerated and free corrosion conditions in laboratory by using electrochemical and surface analytical techniques.

2. Experimental program

2.1. Materials

ASTM C 150 [21] Type-V cement, manufactured by Saudi Kuwaiti Cement Manufacturing Co., was used in all reinforced concrete specimens. Table 1 shows the chemical analysis of the cement.

The coarse aggregate was 19 mm maximum size crushed limestone, with a bulk specific gravity of 2.5 g/cm^3 and an average absorption of 2.45%. As fine aggregate, dune sand of specific gravity 2.6 g/cm^3 and an average absorption of 0.57% was used. All aggregates were washed and dried when procured from the local supplier and were free from fine dust, chloride and sulfate contamination.

The reinforcing steel was procured from a local supplier. Typical composition of the carbon steel used in this study is as follows in percentages: C = 0.38; Si = 0.20; Mn = 1.53; P = 0.020; S = 0.016; Cu = 0.053; Cr = 0.021; Mo = 0.009; Ni = 0.011; Sn = 0.004; V = 0.004; Nb = 0.005; Fe = balance.

Two proprietary inhibitors, M2 and R2, were tested in this study. They were mixed in concrete according to the manufacturers' instructions.

M2 is a proprietary alkanolamine inhibitor that is designed to migrate through concrete to form a protective monolayer on the steel surface. It is used as an admixture in the concrete.

R2 is a water-based inorganic material to inhibit corrosion of steel in concrete. It is added to the batch water.

2.2. Specimen preparation

2.2.1. Reinforced concrete specimens for corrosion

Reinforced concrete specimens of 100 × 65 × 300 mm with a centrally placed 12 mm diameter reinforcing steel bar and 25 mm cover at the bottom were cast. The steel bar, after washing with acetone and distilled water, was insulated at the lower end and at the upper junction with concrete to prevent crevice corrosion. It was, then, centrally placed in the mold before casting the concrete. Group-1 (G-1) specimens were cast without salt contamination with inhibitors M2 and R2. G-2 specimens were contaminated with 1.5% NaCl in the concrete mix. The inhibitors R2 and M2 were mixed with mixing water at a dosage of 5 l/m^3 and 1.2 kg/m^3 of concrete, respectively, as recommended in the manufacturers' catalogs.

Three specimens were cast using each inhibitor. After casting, the specimens were cured under wet burlap for 7 d and then allowed to air-cure under controlled laboratory temperature (22 ± 5°C) for 21 d. Following curing, the specimens were placed in 5% NaCl solution for corrosion.

Table 1
Chemical analysis of the cement

Constituent	Wt%
Silicon dioxide	21.29
Aluminum oxide	3.29
Ferric oxide	5.00
Calcium oxide	64.95
Magnesium oxide	0.95
Sulfur trioxide	2.04
Alkalis	0.60
Loss on ignition	0.86
C_3S	63.30
C_2S	13.28
C_3A	1.93
C_4AF	15.22

2.2.2. Polished steel specimens

Disk-shaped steel specimens measuring 10 mm dia. × 2 mm were prepared from 12 mm diameter reinforcing steel bars. The specimens were polished to 5 μm finish by using SiC papers and alumina paste. The polished specimens were exposed to saturated $Ca(OH)_2$ solution containing salt and inhibitors, and analyzed by electrochemical and surface analytical techniques. Before exposure, the specimens were washed with acetone and distilled water.

2.3. Testing of specimens

2.3.1. Accelerated corrosion specimens

Corrosion of G-1 specimens, which were placed in 5% NaCl solution following 28 d of curing, was accelerated by impressing a +4 V fixed anodic potential for two months or until cracking of the specimens. A DC power source (HP6024A Autoranging PC Power Supply) was used for this purpose. The anodic current was monitored every 2 h throughout the test duration by a computerized data acquisition system connected to the specimens through a resistor. The data were analyzed using a spreadsheet program and the current–time plots were generated. Time to initiation of corrosion was determined from the current–time records. The time to cracking was also monitored by constant visual examination of the specimens at least four times a day.

DC linear polarization resistance (LPR) measurements were also carried out on all the specimens using EG&G PARC Model 350A Corrosion Measurement Console at the following intervals:

(a) Before impressing the anodic potential.

(b) After external cracking was evident, corrosion had initiated, or after two months of impressed anodic potential, whichever occurred first.

For each polarization test, the specimens were transferred to an electrochemical cell containing 5%

NaCl solution and then measurements of polarization resistance were made.

2.3.2. Free corrosion specimens

After 28 d of curing, G-2 specimens were placed in a separate container containing 5% NaCl solution and allowed to corrode freely under laboratory conditions at 22 ± 5°C. Corrosion of the specimens was monitored by measuring the corrosion potential and corrosion current density at periodic intervals. A FLUKE 876B Multimeter was used to measure corrosion potential.

2.3.3. Polished steel specimens

These specimens were exposed to saturated $Ca(OH)_2$ solution containing the following at normal laboratory temperature:

1. NaCl,
2. NaCl + M2, and
3. NaCl + R2

for 48 and 96 h duration.

Following the exposure, the polished surfaces of the specimens were tested for effect of inhibitors on corrosion by anodic polarization and LPR methods. The specimen surfaces were also analyzed to develop an understanding of the inhibition mechanism of these inhibitors in the presence of chloride ions in saturated $Ca(OH)_2$ solution, by using ESCA and Auger spectroscopy (AES).

2.4. Test methods

2.4.1. Linear polarization resistance (LPR)

The corrosion rate of reinforcing steel was evaluated by the LPR method. The corrosion cell consisted of a reference electrode which is located on the concrete surface, a working electrode which is the reinforcing steel embedded in the concrete specimen, and a counter electrode which is placed in the salt solution around the concrete specimen. A stainless steel frame was used as counter electrode. In this technique, the reinforcing steel bar is polarized to ± 20 mV of the open circuit potential (E_{corr}), the potential within which the current varies linearly with applied potential.

The linear polarization resistance, R_p, can be determined from the slope of the plot of applied potential against measured current. The corrosion current density can then be calculated using the Stern–Geary relationship [22] as follows:

$$I_{corr} = B/R_p,$$

where I_{corr} is the corrosion current density ($\mu A/cm^2$), R_p is the polarization resistance ($k\Omega\,cm^2$), $B = (\beta_a\beta_c)/2.3(\beta_a + \beta_c)$, where β_a and β_c are the anodic and cathodic Tafel constants, respectively. For steel in aqueous media, values of β_a and β_c equal to 120 mV are normally used. However, in the absence of sufficient data on β_a and β_c for steel in concrete, a value of B equal to 52 mV for steel in passive condition and a value equal to 26 mV for steel in active condition are normally used. Gonzalez et al. [23] have demonstrated a good correlation between corrosion rates determined by the LPR technique and weight loss measurements for active and passive states of corrosion of steel in concrete. The corrosion rate can be determined by using the following relationship [22]:

$$\text{Corrosion rate (mpy)} = (0.13 I_{corr}\,\text{EW})/d,$$

where I_{corr} is the corrosion current density ($\mu A/cm^2$), EW is the equivalent weight of steel, and d is the density of steel.

For polished specimens, the LPR method was similar to that detailed above (Section 2.3.2, first paragraph) except that a standard corrosion cell was used which is fitted with a standard size disk specimen holder which exposes 100 mm^2 area of the specimen surface and a stainless steel rod for the counter-electrode.

2.4.2. Anodic polarization

Anodic polarization tests were run for control- and inhibitor-treated polished steel specimens. The control specimen was immersed in saturated $Ca(OH)_2$ solution containing 5% NaCl for 48 and 96 h at 22 ± 5°C. The other specimens were immersed in saturated $Ca(OH)_2$ solution containing 5% NaCl + M2 or R2 inhibitors at recommended concentrations of 5 l/m^3 and 1.2 kg/m^3 of solution, respectively. The tests were carried out under anodic potentiodynamic conditions. Starting at the rest potential (E_{corr}), the specimens were polarized towards higher anodic potentials and the corresponding current density (I) was measured automatically. The results were represented as potential–current density plots.

2.4.3. AC impedance spectroscopy

AC impedance measurements were made for one specimen from each batch at the rest potential, before cracking and after cracking, by using Solatron Frequency Response Analyzer (FRA) Model 1250.

The AC impedance spectroscopy provides information on the active–passive behavior and dielectric properties of the metal oxide formed on the steel surface. The impedance technique can also be used to establish the diffusion and migration behavior of the ions towards the reinforcing steel surface.

The AC impedance tests were carried out at the following test conditions:

(a) Amplitude 10 mV.
(b) Sweep from 50 kHz to 1 mHz.
(c) DC potential E_{corr}.
(d) A 4 steps per decade on the log scale sweep.
(e) A delay of 3 s between frequencies.

The AC impedance data were presented in the form of Nyquist and Bode plots. The results were analyzed by elaborating on models of the corresponding equivalent circuit to extract factors such as charge transfer resistance (R_{ct}) relating to the corrosion mechanisms and the corrosion rate.

2.4.4. Surface analyses by electron spectroscopy for chemical analysis (ESCA) and AES

ESCA spectra were generated for four steel specimens, each of which was exposed to one of the following environments:

- 5% NaCl solution,
- saturated $Ca(OH)_2$ solution containing 5% NaCl,
- saturated $Ca(OH)_2$ solution containing 5% NaCl + M2, and
- saturated $Ca(OH)_2$ solution containing 5% NaCl + R2.

For this purpose Perkin Elmer PHI 5300 ESCA System was used with a Mg anode operated at 13 kV and 23 mA. The base pressure of the system was 2×10^{-8} Torr during data collection. The ESCA spectra were taken from samples in their as-received state.

The AES was obtained for only two of the steel samples which were exposed to saturated $Ca(OH)_2$ solution containing 5% NaCl + M2 or saturated $Ca(OH)_2$ solution containing 5% NaCl + R2, respectively. For this purpose Perkin Elmer PHI 600 Scanning Auger Multiprobe was used at a 3 kV beam and beam current of 50–60 nA. To avoid charging, both samples were placed on the sample holder with the help of copper clips.

3. Results and discussions

3.1. Accelerated corrosion tests

The time–current curves for the specimens made with plain concrete and with corrosion inhibitors M2 and R2 are shown in Figs. 1–3, respectively. From Figs. 1–3, it is seen that the current requirement for the specimens are in the order of R2 < M2 < control, which indicates the effectiveness of these inhibitors right from the beginning. The current requirements for the control specimens varied from 11 to 27 mA during 180 h of monitoring period. The large dispersion observed in the current variation could be due to the quality of concrete in the specimens. The current variation was 9–20 mA for M2 and 6–8 mA for R2. The inhibitor R2 was a better performer than M2 throughout the monitoring period and after cracking.

The time–current curves for specimens with M2 indicate that the time-to-initiation of corrosion in the three specimens ranged from 90 to 95 h. The time–current curves for specimens with R2 indicate corrosion initiation after about 380 h in specimen 1. A time period of about 370 h can be assumed for specimen 2 since a significant change in the current requirement is indicated

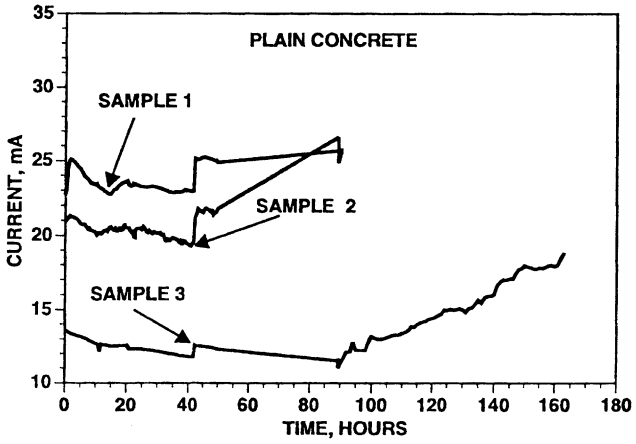

Fig. 1. Time–current curves for plain concrete specimens (control).

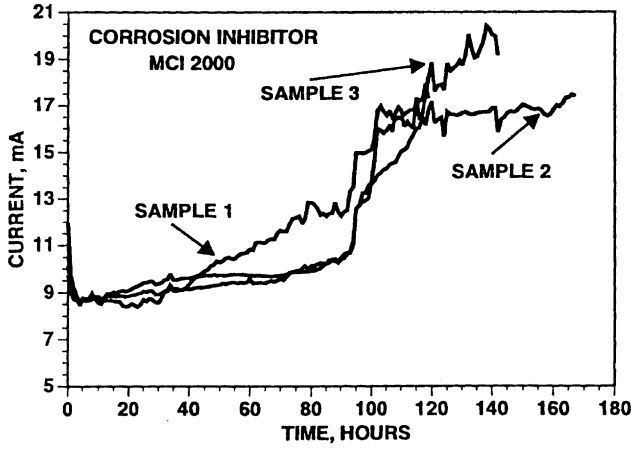

Fig. 2. Time–current curves for concrete specimens incorporating M2.

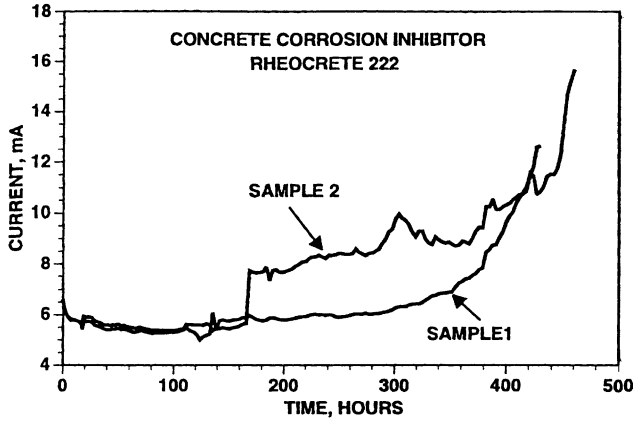

Fig. 3. Time–current curves for concrete specimens incorporating R2.

Table 2
Polarization current, corrosion rates, and charge transfer resistance

Specimen	Polarization current (mA) after application of +4 V	CR (mpy) before application of +4 V	CR (mpy) after cracking of +4 V imposed specimen	Ave. R_{ct} (Ω cm^2) after cracking
Control	19.1	0.123	3.583	8.5
R2	6.4	0.071	3.084	15.5
M2	10.6	0.176	2.780	17.9

after 370 h. From Figs. 1–3, the time-to-cracking of plain concrete specimens was estimated to be 90, 90, and 100 h with an average of 93 h. The average time-to-cracking of the concrete specimens made with M2 and R2 inhibitors were 93 and 375 h, respectively. The time-to-cracking was taken as the point where current requirement increased significantly on the curves.

The corrosion rates of steel in the plain cement concrete and in the concretes made with inhibitors were determined before and after application of the impressed potential. The corrosion rates of steel before application of the anodic potential are presented in Table 2. The average corrosion rate of steel in the plain concrete specimens was 0.123 mils per year (mpy). The corrosion rates of steel in the concrete specimens made with M2 and R2 inhibitors were 0.176 and 0.071 mpy, respectively, before application of anodic potential.

The corrosion rates of steel after cracking of the concrete specimens are shown in Table 2. The corrosion rate of steel in cracked plain concrete specimen was 3.58 mpy, whereas the corrosion rates of steel in specimens containing M2 and R2 inhibitors were 2.78 and 3.08 mpy, respectively.

3.2. Freely corroding specimens

Figs. 4–6 show the corrosion potential–time curves for freely corroding specimens. The corrosion potential–time curves for steel in the plain concrete specimens, shown in Fig. 4, indicate possibility of active corrosion even before exposure to the salt solution, i.e., the potentials are more negative than the −270 mV saturated calomel electrode (SCE). According to ASTM C 876 [24] potentials more negative than −350 mV copper–copper sulfate electrode, i.e., −270 mV SCE indicate a 90% probability of active corrosion. The potentials in all the three specimens continue to decrease (become more negative) at an exposure period of 7 d. After 7 d, these readings are more or less stable. The corrosion potential–time curves for steel in the concrete specimens

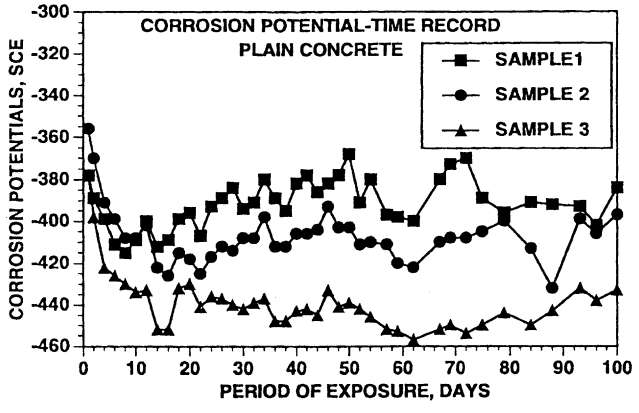

Fig. 4. Corrosion potential–time curves for plain concrete specimens.

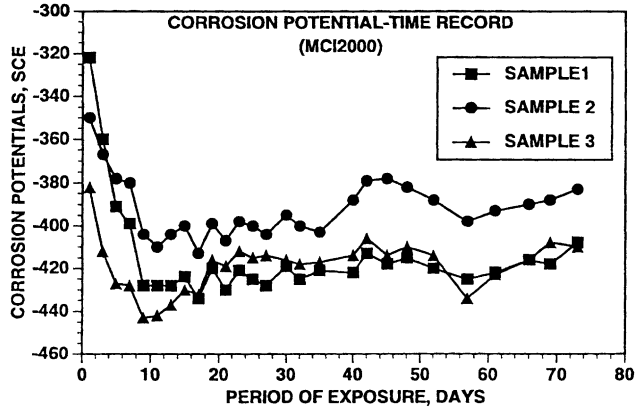

Fig. 5. Corrosion potential–time curves for concrete specimens incorporating inhibitor, M2.

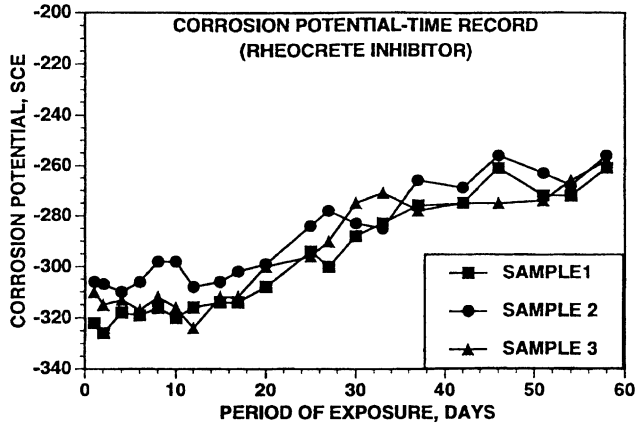

Fig. 6. Corrosion potential–time curves for concrete specimens incorporating inhibitor, R2.

containing inhibitor M2 are shown in Fig. 5. These data indicate a trend similar to that observed in the plain concrete specimens shown in Fig. 4. The corrosion potential–time curves for steel in the concrete specimens mixed with R2 are plotted in Fig. 6. The potential values of steel in all the three specimens made with this inhibitor were more negative than −270 mV at the time of exposure. However, with increasing periods of exposure, the potential values tended to increase (become less negative). The potential values in these specimens started crossing the ASTM C 876 threshold potential of −270 mV SCE after about 36 d of exposure and increased with the exposure period.

The average values of the corrosion potentials on steel bars in all the specimens were more or less similar with the exception of the specimens made with inhibitor R2. The corrosion potentials of the specimens with R2 were more positive than corrosion potentials of the other specimens right from the beginning of exposure.

The corrosion rates of steel bars in the contaminated and freely corroding specimens are shown in Fig. 7. The corrosion rates of steel in the plain concrete and those made with inhibitor R2 were much less than the corrosion rate of steel in the concrete specimens made with inhibitor M2. With time of exposure, the rate of corrosion of steel in the control specimens increased, while in R2 specimens it remained almost constant. After 55 d of exposure to accelerated corrosion, the rate of corrosion of reinforcing steel bar was 1.3, 1.6 and 0.75 mpy in the plain concrete specimens, in specimens with inhibitor M2, and in specimens containing inhibitor R2, respectively.

3.3. AC impedance study

The AC impedance study of the specimens before cracking did not produce meaningful results. Therefore,

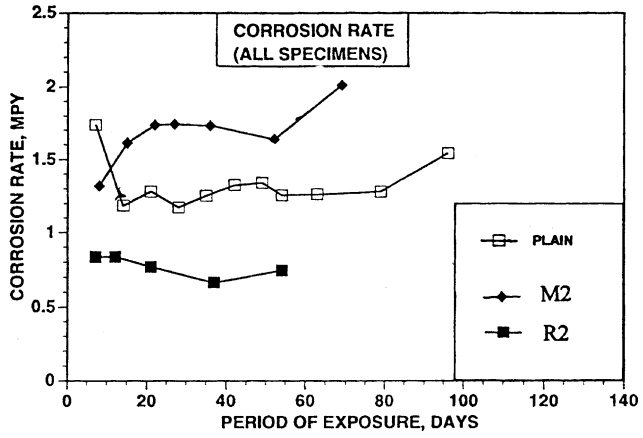

Fig. 7. Corrosion rate of steel in chloride-contaminated (freely corroding) concrete specimens.

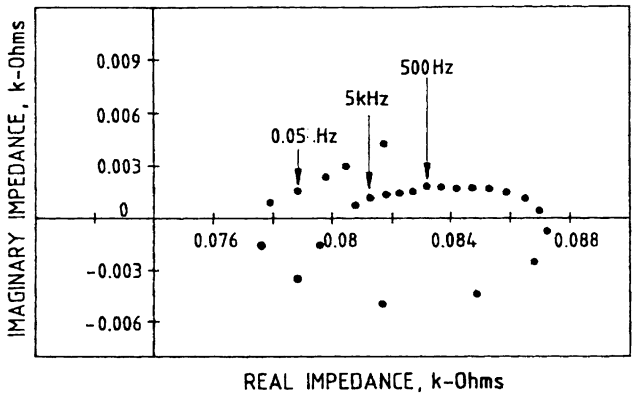

Fig. 8. Nyquit plot for uncoated specimen.

this study was carried out for the accelerated corrosion specimens after cracking. The measurements were made at E_{corr} after the concrete samples cracked.

In the case of plain rebar (uncoated) sample (Fig. 8), the spectrum exhibits a high-frequency capacitive loop (corresponding to C_{dl}–R_{ct} circuit) and an inductive loop at lower frequency (e.g. between 15.8 and 0.5 Hz). The behavior at frequencies lower than 0.5 Hz is consistent with the absorption and surface relaxation processes of species that, in this case, are favorable to corrosion processes.

The data on charge transfer resistance (R_{ct}) obtained from impedance for the different inhibitors are shown in Table 2. The higher the R_{ct} value, the lower the corrosion rate, thus, according to R_{ct} values, the corrosion rate of the inhibited specimens after cracking appear to be in the following order: control > R2 > M2. This is probably due to deterioration of inhibitive effect of R2 after cracking of concrete.

3.4. Anodic polarization

Fig. 9 shows the anodic polarization curves. The results of LPR are presented in Table 3. The curves and results show that, although both of the inhibitors retard corrosion of the steel specimens, R2 is more effective than M2 in doing so. After 48 h of immersion the corrosion rates were 2.49, 5.00 and 0.52 mpy in solutions of 5% NaCl containing $Ca(OH)_2$, $Ca(OH)_2 + M2$ and $Ca(OH)_2 + R2$, respectively. During the first two days of immersion, M2 had adverse effect on the corrosion of steel. After 96 h, however, corrosion rates of steel bars were measured to be 14.30, 12.40 and 2.67 mpy in solutions of 5% NaCl containing $Ca(OH)_2$, $Ca(OH)_2 + M2$ and $Ca(OH)_2 + R2$, respectively. The results indicate that R2 is a more effective inhibitor than M2 in retarding corrosion of steel in the presence of chloride ions. This is also evident from Fig. 9 where R2 displays a steeper anodic polarization curve than M2.

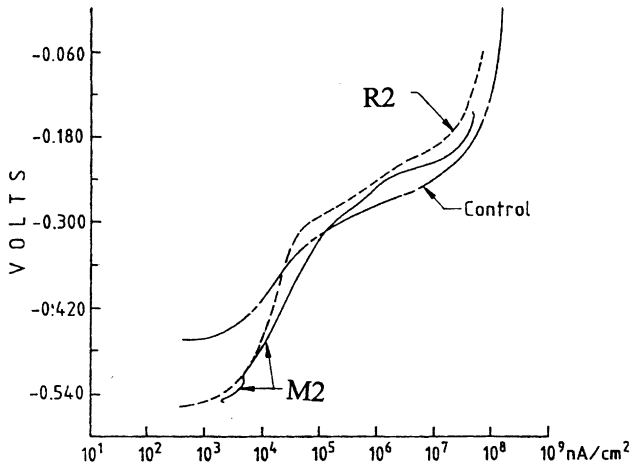

Fig. 9. Anodic polarization curves and effect of inhibitors after 96 h exposure of steel specimens to the inhibitors.

3.5. Study of inhibition mechanism

3.5.1. ESCA analysis

The ESCA survey spectra was collected from the four specimens exposed to four different environments. The corresponding typical multiplex spectra for iron are presented in Figs. 10–13. The binding energies of the peaks of the spectra given in these figures have not been corrected for charging. Binding energy (BE) values, which have been charge-compensated, are presented in Table 4. Atomic concentrations of elements on the surface layer of the specimens are presented in Table 5.

As seen from Table 4, the features that are due to carbon, the oxygen group (oxide, hydroxide, water) are common to all spectra, while the features due to nitrogen and silicon (possibly silicate) are observed only for the samples exposed to M2 and R2, respectively. The amounts of nitrogen and silicon are quite small.

Except for the presence of calcium, the surfaces treated either with 5% NaCl, 5% NaCl + sat. $Ca(OH)_2$, or 5% NaCl + sat. $Ca(OH)_2$ + M2 are rather similar from the point of view of the species on the surface. This is not to say, however, that there is practically no difference. The signal strengths of Na, Cl, and Fe have all diminished for surfaces additionally treated with $Ca(OH)_2$ compared with those treated either with 5% NaCl or with 5% NaCl + sat. $Ca(OH)_2$ + M2. The low-energy C 1s peak at about 285 eV is common to all specimen surfaces inspected. It is probably due to contamination of the specimens from the atmosphere.

The multiplex spectra of O 1s, Fe $2p^{3/2}$ and Cl 2p obtained from the steel surface treated with 5% NaCl indicate that the surface layer most probably consisted of several iron oxides such as γ-Fe_2O_3, Fe_3O_4, iron oxyhydroxide (FeOOH), and iron chloride ($FeCl_2$). This is consistent with the already published results [25–28]. Foley et al. [26] reported development of Fe_3O_4 and

Table 3
Results of linear polarization resistance tests

Specimens	After 48 h		After 96 h	
	R_p (Ω cm^2)	Corr. rate (mpy)	R_p (Ω cm^2)	Corr. rate (mpy)
Control	7552	2.49	1039	14.30
M2	5148	5.00	1743	12.40
R2	12 350	0.52	8108	2.67

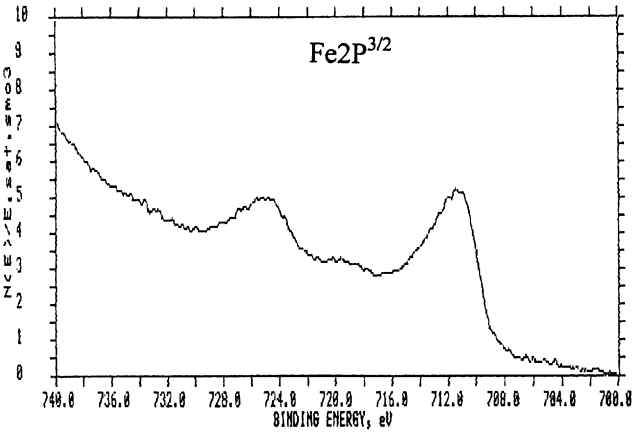

Fig. 10. ESCA multiplex spectra for Fe 2p of steel specimen exposed to 5% NaCl solution.

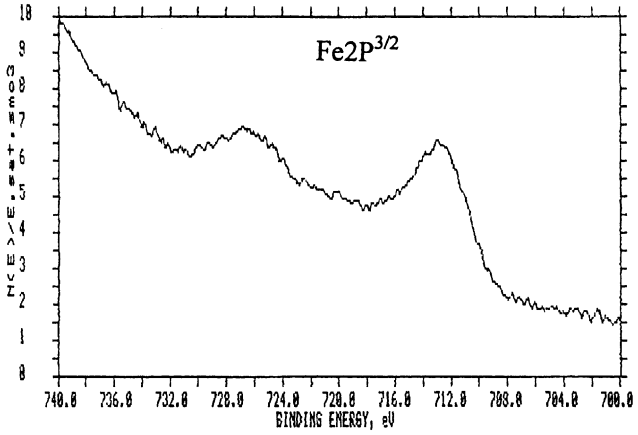

Fig. 11. ESCA multiplex spectra for Fe 2p of steel specimen exposed to 5% NaCl + sat. $Ca(OH)_2$ solution.

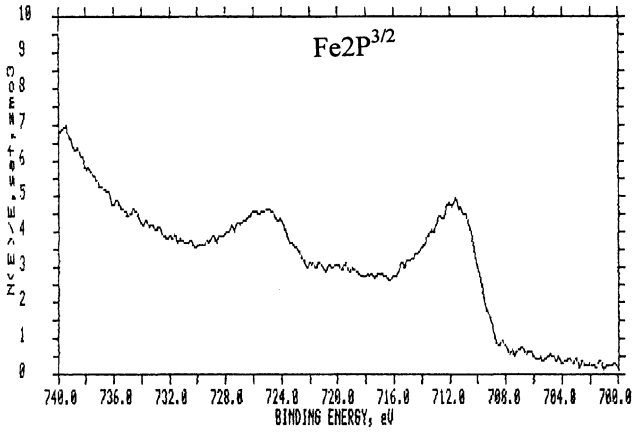

Fig. 12. ESCA multiplex spectra for Fe 2p of steel specimen exposed to 5% NaCl + sat. $Ca(OH)_2$ + M2 solution.

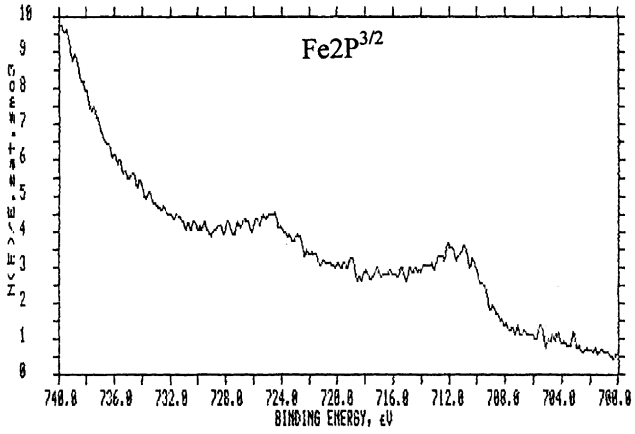

Fig. 13. ESCA multiplex spectra for Fe 2p of steel specimen exposed to 5% NaCl + sat. $Ca(OH)_2$ + R2 solution.

FeOOH on steel surfaces outside the passive region, whereas Sato et al. [27] reported development of γ-FeOOH and γ-Fe_2O_3 in acidic environment. According to Allam et al. [28], $FeCl_2$ and $FeCl_3$ could form on the steel surface in the presence of NaCl under atmospheric conditions.

The O 1s, Fe $2p^{3/2}$ and Cl 2p multiplex spectra profiles indicate that, with the introduction of sat. $Ca(OH)_2$ in the environment, the compounds on the steel surface become predominantly FeOOH with some γ-Fe_2O_3 and $FeCl_3$. Zacroczymski et al. [29] and Montemor et al. [30] also reported the formation of FeOOH on pure iron in NaOH solution and on mild steel in chloride-ion-containing environment, respectively. The lower corrosion rate of the steel specimens in 5% NaCl + sat. $Ca(OH)_2$ compared to the corrosion rate in 5% NaCl [31] is evidenced with weak oxygen and chloride peaks in the respective multiplex spectra obtained in the former case (Table 4).

After the treatment with organic inhibitor M2, in addition to 5% NaCl + sat. $Ca(OH)_2$, three more C 1s peaks (other than the peak at 285.7 eV) with higher binding energy were identified on the surface. The high-energy C 1s peaks are attributable to the film formation by the organic inhibitor on the steel surface. The O 1s and Fe $2p^{3/2}$ peak profiles, in this case, indicate that the steel surface is probably composed of mainly Fe_2O_3 with some Fe_3O_4 and $FeCl_2$. The steel surface also showed high-energy peaks for O 1s (at 532.1 eV) and Cl $2p^{3/2}$ (at 200.2 eV) in corresponding multiple spectra. These high-energy peaks could be due to organic oxygen and chlorine in the composition of M2. Increased oxygen and chlorine on the steel surface treated with M2 is probably the cause of inferior performance of this inhibitor compared to inorganic inhibitor R2.

The Fe $2p^{3/2}$ and broad O 1s peak profiles obtained from steel surface exposed to inorganic inhibitor R2, in addition to 5% NaCl + sat. $Ca(OH)_2$, indicate the presence of mainly Fe_2O_3, Fe_3O_4, FeO and $Fe(OH)_2$ on the surface. The weak high-energy O 1s peak (at 533.6

Table 4
Charge-compensated binding energies (eV)

Sample	C 1s	O 1s	Na 1s	Fe $2p^{3/2}$	Cl 2p	Ca $2p^{3/2}$	N 1s	Si 2p
5% NaCl	285.6	529.7 531	1071.4	710.1	199.0	None	None	None
5% NaCl + sat. $Ca(OH)_2$	285.7 290	528.8 weak 531.5 534.5 weak	Broad and weak	711.6	199.0 weak	347.4	None	None
5% NaCl + sat. $Ca(OH)_2$ + M2	285.7 286.7 291.3 291.9	529.3 530.6 532.1	1072.4	710.2	199.0 200.2	348.1	398.7	None
5% NaCl + sat. $Ca(OH)_2$ + R2	284.5 Reference	529.3 weak 531.1 533.6 weak	None	709.9	None	347.5	None	102.3

eV) could be due to SiO_2 in the composition of inhibitor R2. The chlorine and sodium were not detected on the steel surface in this case. The observations are consistent with the better protection shown by inorganic inhibitor R2 against corrosion of steel in sodium chloride environment. The inorganic inhibitor is probably reacting with the chloride and sodium ions in the solution, preventing them from reaching the steel surface, and thus protecting the surface against corrosion.

3.5.2. Scanning Auger multiprobe (SAM) analysis (AES)

Figs. 14 and 15 give the AES spectra obtained from the surfaces exposed to M2 and R2, respectively. The elements observed on each surface are also indicated on the figures. A common feature of the AES spectra from these surfaces is the dominance of the signal due to carbon. Calcium is also seen to be present on each surface. On the other hand, the AES signal attributed to iron is seen to be weaker for the surface treated with R2 than for the surface treated with M2, which suggests that the R2 protects the surface from corrosion more than M2 does. Finally it should be pointed out that this conclusion is consistent with that reached earlier using ESCA.

The surface analysis (Table 5) of the inhibitor-treated steel specimens using ESCA and AES showed that the steel treated with R2 did not have any chloride or sodium ion in the surface layer. It was weak in iron, oxygen and silicon content. The indications are such that R2 might have modified the passive film on the surface to consist mainly of Fe_2O_3. Also, R2 might have reacted with chloride ions in the vicinity of the metal surface to prevent them from reaching the surface, whereas M2 has a nitrogen group in its composition which probably modified iron oxide on the steel surface to mainly Fe_2O_3 in the presence of saturated calcium hydroxide and at the same time formed a protective film on the steel surface. However, the organic chlorine and oxygen in the composition of M2 is probably one of the reasons for its inferior performance compared to R2.

3.6. Performance rating of inhibitors

The performance ratings of inhibitors M2 and R2 are summarized in Table 6. The results show that R2 is a much better performer as inhibitor than M2 in saturated $Ca(OH)_2$ solution, in the presence of chloride ions. The effectiveness of R2 in retarding corrosion of steel is superior both in concrete as well as without concrete. The

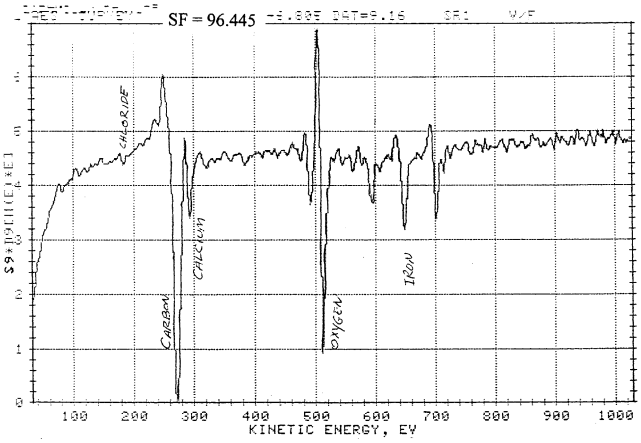

Fig. 14. AES spectra obtained from the surfaces exposed to M2.

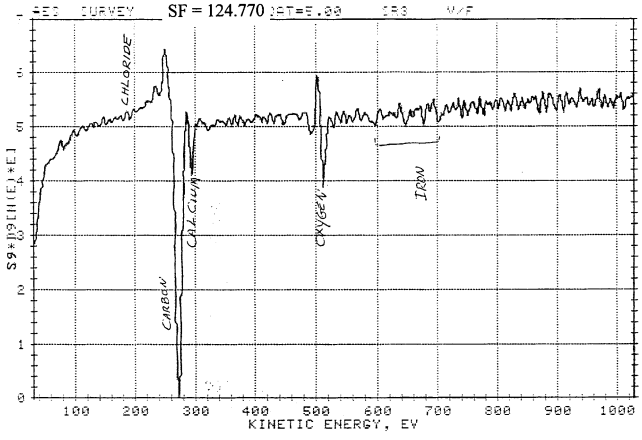

Fig. 15. AES spectra obtained from the surfaces exposed to R2.

Table 5
Atomic concentrations of elements on the surface of steel specimens

Element	5% NaCl concentration (%)	5% NaCl + sat. $Ca(OH)_2$ concentration (%)	5% NaCl + sat. $Ca(OH)_2$ + M2 concentration (%)	5% NaCl + sat. $Ca(OH)_2$ + R2 concentration (%)
Cl 2p	5.26	1.05	5.63	–
Na 1s	2.05	0.83	2.85	–
Ca 2p	–	3.69	3.02	1.60
Fe 2p	6.64	3.98	4.54	0.46
O 1s	28.85	27.10	33.25	14.52
C 1s	57.20	63.31	50.70	82.36
Si 2p	–	–	–	1.05

Table 6
Performance evaluation of the inhibitors

Material	Acc corr. rate before imp. potential		Polarization current after impressing +4 V		Cracking time		Acc corr. rate after cracking		Free corr. rate		AC impedance after cracking		Anodic polarization corr. rate 48 h		Anodic polarization corr. rate 96 h	
	mpy	Perf.	mA	Perf.	hr	Perf.	mpy	Perf.	mpy	Perf.	R_{ct}	Perf.	mpy	Perf.	mpy	Perf.
Control	0.123	1.00	19.1	1.00	106	1.00	3.583	1.00	1.35	1.00	8.5	1.00	2.49	1.00	14.30	1.00
M2	0.176	0.70	10.6	1.80	135	1.27	2.780	**1.29**	1.70	0.79	17.9	**2.10**	5.00	0.49	12.40	1.15
R2	0.071	**1.73**	6.4	**2.98**	434	**4.09**	3.084	**1.16**	0.70	**1.93**	15.5	**1.82**	0.52	**4.79**	2.67	**5.36**

results obtained from accelerated corrosion under impressed potential and free corrosion of contaminated reinforced concrete specimens clearly demonstrate the higher effectiveness of R2 as inhibitor in the presence of chloride ions. The only time when M2 shows better performance is after the concrete cover over the steel bar cracks as shown by both DC LPR and AC test results. Probably cracking induces unrepairable damage to the passive layer formed on steel surface in the presence of R2, thus leading to higher corrosion in R2-containing specimens than in specimens with M2. The superior corrosion inhibiting characteristics of R2 over M2 were also shown by ESCA and AES analysis of steel surfaces. According to cracking time the R2 containing concrete performs four times better than the control specimen. According to anodic polarization results, the steel surface treated with R2 solution for 96 h performed five times better than the control steel surface in the presence of chloride ions.

4. Conclusions

From the data developed in this study, the following conclusions are made:

1. The time-to-cracking in uncontaminated concrete specimens made with inhibitors M2 and R2 was higher than that of the control concrete specimens. While the increase in the time-to-cracking in the concrete specimens incorporating M2 was marginal, a significant improvement in the corrosion-resisting characteristics of concrete incorporating R2 was indicated over the control specimens. The time-to-cracking in concrete specimens incorporating M2 and R2 was 1.3 and 4 times higher in order of magnitude than that in the control specimen, respectively.
2. The data on time-to-cracking in the uncontaminated concrete specimens and the corrosion rate of steel in the contaminated concrete specimens indicate the better performance of inhibitor R2 in retarding reinforcement corrosion, both in terms of time to initiation of corrosion and corrosion propagation.
3. The better performance of inhibitor R2 over M2 was also shown by electrochemical investigation on steel specimens immersed in an inhibitor containing 5% $NaCl$ + saturated $Ca(OH)_2$ solutions. After 96 h exposure to inhibitor containing solution the corrosion rates were in the following ratio: control $>$ M2 $>$ R2 $= 5.4 > 4.6 > 1$.
4. The surface analysis indicated that R2 most probably modified the passive film on the steel surface as well as reacted with chloride ions in the vicinity of the metal and stopped them from reaching the surface, whereas M2, which has nitrogen group in its composition, might have modified the passive film on the

steel surface and at the same time formed a film on the surface to protect the steel against corrosion in the presence of chloride ions. Organic oxygen and chlorine in the composition of M2 could be one of the causes of its inferior performance compared to that of R2.

Acknowledgements

The authors wish to acknowledge the support of King Fahd University of Petroleum and Minerals, Research Institute, Center for Engineering Research, for this work. Also, Mr. M.A. Romano's contribution to interpretation of ESCA and AES results are greatly appreciated.

References

[1] Saricimen H, Al-Tayyib AJ, Maslehuddin M, Shamim M. Concrete deterioration in high chloride-sulfate environment and repair strategies. American Concrete Institute Special Publication SP-128, Detroit, 1991. p. 19–34.
[2] Saricimen H. Durable concrete research for aggressive environment. In: Proceedings, CREATING WITH CONCRETE, An International Congress, September 1999; Dundee.
[3] Saricimen H. Concrete durability problems in the Arabian Gulf region – a review. In: Proceedings of 4th International Conference on Deterioration and Repair of Reinforced Concrete in the Arabian Gulf, October 1993; Manama, Bahrain. p. 943–59.
[4] Saricimen H, Allam IM, Maslehuddin M, Al-Mana AI. Effect of atmospheric corrosion on mechanical properties of reinforcing steel bars. In: Proceedings of 6th M.E. Corrosion Conference, January 1994; Manama, Bahrain. p. 563–79.
[5] Griffin DF. Corrosion inhibitors for reinforced concrete. In: Corrosion of metals in concrete. ACI SP-49, Detroit, 1975. p. 95–102 [cited in [9]].
[6] Craig RJ, Wood LE. Effectiveness of corrosion inhibitors and their influence on the physical properties of Portland cement mortars. Highw Res Rec 1970;328:77 [cited in [9]].
[7] Treadaway KWJ. Corrosion of steel in alkaline chloride solutions. DSc Thesis, University of Galford, Apr. 1966 [cited in [9]].
[8] Slater JE. Corrosion of metals in association with concrete. ASTM Special Publication No. 818, 1983.
[9] Berke NS. Corrosion inhibitors in concrete. In: Concrete International, July 1991.
[10] Berke NS. Corrosion inhibitors in concrete. Paper No. 445. In: Corrosion/89. Houston: Nace; 1989. p. 10 [cited in [9]].
[11] Treadaway KWJ, Russel AD. In: Highways and Public Works, Sept. 1968, vol. 36. p. 40 [cited in [9]].
[12] Rosenberg AM, Gaidis JM, Kossivas TG, Previte RW. A corrosion inhibitor formulated with calcium nitrite for use in reinforced concrete. In: Tonini DE, Dean Jr. SW, editors. Chloride corrosion of steel in concrete. ASTM STP, 629. 1977. p. 89–99 [cited in [8]].
[13] Arber MG, Vivian HE. Aust J Appl Sci 1961;12:339 [cited in [9]].
[14] Hope BB, Ip AKC. Corrosion inhibitors for use in concrete. ACI Mater J (November–December) 1989. p. 602.
[15] Berke NS, Sundberg KM. The effects of calcium nitrite and microsilica admixtures on corrosion resistance of steel in concrete. In: Proceedings, Paul Klieger Symposium on Performance of Concrete. ACI SP-122, 1990. p. 269.
[16] Virmani YP, Clear KC, Pasco TJ. Time-to-corrosion of reinforcing steel in concrete slabs. vi. 5, Calcium nitrite admixture and epoxy coated reinforcing bars as corrosion protection systems. Report No. FHWA RD-83 012, Federal Highway Administration, Washington, DC, Sept. 1983, p. 71 [cited in [9]].
[17] Berke NS. Effects of calcium nitrite and mix design on the corrosion resistance of steel in concrete (Part 2, Longterm results). In: Corrosion of metals in concrete. Houston: Nace; 1987. p. 134 [cited in [9]].
[18] Tomazawa F, Masuda Y, Tanaka H, Fukushi I, Takakura M, Hori T, Higashi S. An experimental study on effectiveness of corrosion inhibitor in reinforced concrete under high chloride content conditions. Nihon Architecture Society, Oct. 1987 [cited in [9]].
[19] Collins WD, Weyers RE, Al-Qadi IL. Chemical treatment of corroding steel reinforcement after removal of chloride-contaminated concrete. Corrosion 1993;49(1):74.
[20] Prowell BD, Weyers RE, Al-Qadi IL. Evaluation of corrosion inhibitors for the rehabilitation of reinforced concrete structures. Research sponsored by Strategic Highway Research Program and carried out at Virginia Polytechnic Institute and State University, Blacksburg, VA, May 1993 [the paper was provided by the manufacturer of MCI2000].
[21] ASTM C 150. Standard specification for Portland cement. Section 4, Construction, vol. 4.01. Philadelphia: American Society for Testing and Materials; 1992.
[22] Stern M, Geary AL. Electrochemical polarization, No. 1, theoretical analysis of the shape of polarization curves. J Electrochem Soc 1957;104(1):56.
[23] Gonzalez JAA, Feliu S, Andrade C, Rodriguez I. Quantitative measurement of corrosion of reinforcing steels embedded in concrete using polarization resistance measurements. Werkst Korros 1978;29:515–9.
[24] ASTM C 876. Test method for measuring the half-cell potentials of reinforcing steel in concrete. Section 4, Construction, vol. 4.01. Philadelphia: American Society for Testing and Materials; 1992.
[25] Kruger J. Passivity of metals – a material science perspective. Int Mat Rev 1988;33(3):113.
[26] Foley CL, Kruger J, Bechtoldt CJ. J Electrochem Soc 1967;114:944–1001 [cited in [25]].
[27] Sato N, Kudo K, Nishibura R. J Electrochem Soc 1976;123:1419–23 [cited in [25]].
[28] Allam IM, Arlow JS, Saricimen H. Initial stages of atmospheric corrosion of steel in the Arabian Gulf. Corros Sci 1991;32(4):417–32.
[29] Zacroczymski T, Fan C-J, Szklarska-Smialowska Z. Kinetics and mechanics of passive film formation on iron in 0.05 M NaOH. J Electrochem Soc 1985;132(12):2862–7.
[30] Montemor MF, Simoes AMP, Ferreira MGS. Analytical characterization of the passive film formed on steel in solutions simulating the concrete interstitial electrolyte. Corrosion 1998;54(5):347–53.
[31] Saricimen, H., et al. Unpublished data.